X-ray Crystallographic Determination of the Structure of Bovine Lens Leucine Aminopeptidase Complexed with Amastatin: Formulation of a Catalytic Mechanism Featuring a *gem*-Diolate Transition State[†,‡]

Hidong Kim and William N. Lipscomb*

Gibbs Chemical Laboratory, Harvard University, Cambridge, Massachusetts 02138

Received March 30, 1993; Revised Manuscript Received May 11, 1993

ABSTRACT: The structure of the complex of bovine lens leucine aminopeptidase (blLAP) with the slow-, tight-binding inhibitor amastatin has been determined by X-ray crystallography. X-ray diffraction data were collected at −150 °C from a single blLAP–amastatin crystal which under the data collection conditions was of the space group $P6_322$ with unit cell parameters a = 130.3 Å and c = 121.9 Å. The structure of the blLAP–amastatin complex was determined by molecular replacement, using the structure of native blLAP as the starting model. Refinement of the blLAP–amastatin model plus 132 water molecules against data from 10.0- to 2.4-Å resolution resulted in a final structure with a crystallographic residual of 0.198. The binding mode of amastatin is similar to that of bestatin, the structure of whose complex with blLAP has previously been determined. Of particular note, the N-terminus-to-C-terminus orientation of the two bound inhibitors is the same. The two N-terminal residues of amastatin and bestatin occupy the same binding sites, which are most likely S_1 and S'_1. The slow binding of amastatin and bestatin may be partially attributable to a binding mechanism in which the two active site metals are sequentially coordinated by the P_1 amino and hydroxyl groups of these inhibitors. A catalytic mechanism for blLAP is proposed based on the binding modes of amastatin and bestatin and plausible binding modes of a dipeptide substrate and its putative *gem*-diolate transition state which were modeled into the active site of blLAP after the binding mode of amastatin. The proposed catalytic mechanism invokes roles for the catalytic metals in binding and activating the substrate and in stabilizing the transition state. The mechanism also includes roles for Asp-255 as a general base, Arg-336 as an additional electrophilic substrate activator and transition state stabilizer, and Lys-262 as a proton shuttle.

Leucine aminopeptidase (LAP)[1] is a cytosolic aminoexopeptidase which cleaves the N-terminal residue from polypeptide substrates. The three-dimensional structures of LAP isolated from bovine lens (blLAP) and its complex with the inhibitor bestatin have recently been determined by X-ray crystallography (Burley et al., 1990, 1991, 1992; Kim, et al., 1993). As part of our continuing X-ray crystallographic investigations of blLAP, we now report the X-ray structural determination of blLAP complexed with the inhibitor amastatin.

Native blLAP is a hexamer of total molecular weight 324 000. Each of the six identical protomers is a single-chain protein of 487 amino acid residues (MW 54 000) and two Zn^{2+}s which are crucial in catalysis (Melbye & Carpenter, 1971; Carpenter & Vahl, 1973). The amino acid sequence of blLAP, determined by both protein and DNA sequencing (Cuypers et al., 1982; Wallner and Taylor, unpublished data), appears to be well conserved in LAPs and some other aminoexopeptidases from different organisms. Although the amino acid sequences of the human and porcine LAPs have not been reported, immunodiffusion tests have shown that the differences in amino acid sequences between bovine and porcine LAPs, and bovine and human LAPs, are 8.5% and 19%, respectively (Taylor et al., 1984a,b). The amino acid sequence of blLAP also shows an overall 31% identity of residues and a 52% identity of residues in the C-terminal domain to that of the *pepA*-encoded aminopeptidase from *Escherichia coli* and *Salmonella typhimurium* (Stirling et al., 1988, 1989). In blLAP, the C-terminal domain contains the active site (Burley et al., 1990, 1991, 1992; Taylor et al., 1992). Furthermore, the residues involved in metal coordination and inhibitor binding in blLAP, as revealed by the structure of the blLAP–bestatin complex, are conserved in the *pepA*-encoded aminopeptidase (Burley et al., 1992). Such high sequence homology strongly suggests similarities in structure among these aminoexopeptidases. A database of sequence homology-derived protein structures showed that for very long sequence alignment lengths, ~80 residues or longer, a 25% sequence identity is sufficient to infer structural homology (Sander & Schneider, 1991). Because of the apparent similarity not only in overall primary structure, but also in key active site residues among these aminoexopeptidases, it may be that conclusions drawn from structural studies of blLAP can be applied to other aminoexopeptidases as well.

The competitive, noncovalent LAP inhibitors amastatin and bestatin (Umezawa et al., 1976; Aoyagi et al., 1978) (Figure 1) have been widely studied since they are among the strongest known inhibitors of LAP. The K_i of bestatin is 1.3×10^{-9} M with respect to blLAP (Taylor et al., 1993), and the K_i of amastatin is 2×10^{-7} M with respect to porcine kidney LAP (pkLAP) (Rich et al., 1984). Numerous studies have sought

† Support for this research was provided by a grant (GM-06920) to W.N.L. from the National Institutes of Health and a National Science Foundation Predoctoral Fellowship to H.K. Additional support was provided by a Pittsburgh Supercomputing Center grant (1 P41 RR06009) from the National Institutes of Health National Center for Research Resources.

‡ This structure has been deposited in the Protein Data Bank under filename 1BLL.

* To whom correspondence should be addressed.

[1] Abbreviations: LAP, leucine aminopeptidase; blLAP, bovine lens leucine aminopeptidase; pkLAP, porcine kidney leucine aminopeptidase; LV, L-leucyl-L-valine; LVTS, putative *gem*-diolate transition state for the proteolysis of L-leucyl-L-valine; MPD, 2-methyl-2,4-pentanediol; rms, root mean square; F_o and F_c, observed and calculated structure factors.

0006-2960/93/0432-8465$04.00/0

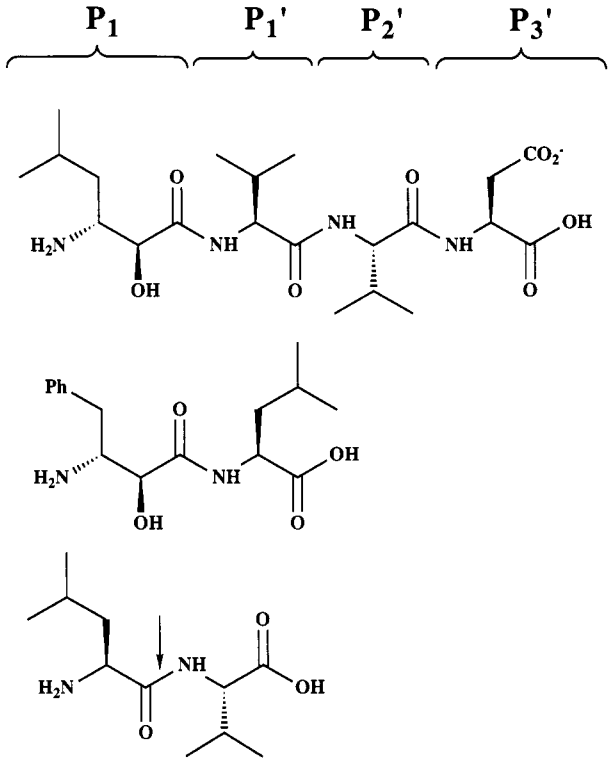

FIGURE 1: (Top) The LAP inhibitor amastatin [(2*S*,3*R*)-3-amino-2-hydroxy-5-methyl-hexanoyl-L-valyl-L-valyl-L-aspartic acid]. (Middle) The LAP inhibitor bestatin [(2*S*,3*R*)-3-amino-2-hydroxy-4-phenylbutanoyl-L-leucine]. (Bottom) The dipeptide substrate of LAP L-leucyl-L-valine (LV). The arrow indicates the scissile bond of LV. The residual portions of the ligands are also indicated.

to determine the binding modes of these inhibitors which have been assumed to be transition-state analogues for LAP-catalyzed proteolysis. Particular interest has been placed on the interaction of the nonproteinaceous hydroxyl group of the P_1 residue[2] with the active site metals (Nishino & Powers, 1979; Nishizawa et al., 1977; Rich et al., 1984; Ocain & Rich, 1988; Harbeson & Rich, 1988; Gordon et al., 1988). The structure of the blLAP–amastatin complex shows that the binding mode of amastatin, a tetrapeptide analogue inhibitor, is similar to that of bestatin, a dipeptide analogue inhibitor (Burley et al., 1991, 1992; Kim et al., 1993). The N-terminus-to-C-terminus orientation of both bound inhibitors is the same and most likely also applies to substrates and reaction intermediates of blLAP.

On the basis of the binding mode of amastatin, the dipeptide substrate L-leucyl-L-valine and its putative *gem*-diolate transition state were built into the active site of blLAP. These modeled binding modes suggest a plausible general base mechanism of catalysis. The mechanism proposed from these crystallographically determined binding modes of amastatin and bestatin and the modeled binding modes of a substrate and its transition state includes important catalytic roles for the two active site metals which are known to affect blLAP catalysis (Hanson & Frohne, 1976; Carpenter & Vahl, 1973; Thompson & Carpenter, 1976; Allen et al., 1983). In addition to the Zn^{2+}s, amino acid residues of blLAP certainly also have some roles in catalysis. One enzymic residue implicated in catalysis by the blLAP–amastatin structure is Arg-336. The side chain of this residue clearly adopts two different conformations in the structure of the complex. One conformation, which appears to be more catalytically productive than the other, allows the guanidinium group of the Arg-336 side chain to interact with the scissile carbonyl oxygen of the substrate in the modeled binding mode of the substrate. This modeled interaction may indicate that Arg-336 acts as an electrophile in catalysis to polarize the scissile carbonyl for nucleophilic attack.

Amastatin and bestatin are also slow-binding inhibitors of LAP (Wilkes & Prescott, 1985). A possible mechanism for the slow binding of these inhibitors is suggested by the binding mode of amastatin in light of the recent reassignment of the two metal binding sites in blLAP. The X-ray crystal structure of the Zn^{2+}–Mg^{2+} metallohybrid blLAP showed that Zn-488 occupies the readily exchanging metal site 1 and Zn-489 occupies the more tightly binding metal site 2 in native blLAP (Kim & Lipscomb, 1993). This result reversed the previous presumptive assignment of the two Zn^{2+}s which was based on the structure of native blLAP (Burley et al., 1992). The arrangement of the metals as predicated by the new assignment of the metal binding sites suggests a possible late stage binding mechanism involving sequential coordination of the metals by amastatin and bestatin which may contribute to the slow binding of these inhibitors. This binding mechanism is consistent with low temperature kinetic studies which have indicated that there are at least two distinct pre-steady-state intermediates in the hydrolysis of a dansyl dipeptide substrate by pkLAP (Van Wart & Lin, 1983; Lin et al., 1988b).

MATERIALS AND METHODS

blLAP was isolated from bovine calf eye lenses according to the method of Carpenter (Allen et al., 1983). The lenses were purchased from Pel-Freez Biologicals and were received packed on wet ice, 1 day after slaughter. The isolated blLAP was further purified by gel filtration chromatography. Typically, 1 mL of 10 mg/mL protein solution in a storage buffer of 50 mM Tris/50 μM $ZnSO_4$/200 mM NaCl/pH 7.8 was separated over a 55 cm × 2 cm (diameter) Sephadex G-100 column using the same storage buffer at a flow rate of 0.3 mL/min at 4 °C. Fractions of 1 mL were monitored for protein by UV absorption at λ = 280 nm, and those fractions containing the purified blLAP as judged by 15% SDS-PAGE were pooled and concentrated to 7 mg/mL protein in the storage buffer.

Crystals of the blLAP–amastatin complex suitable for X-ray diffraction studies were grown from solutions of blLAP–amastatin complex by vapor diffusion and macroseeding (Eichele et al., 1979; Thaller et al., 1981) at room temperature. A 200-fold molar excess of amastatin hydrochloride, purchased from Sigma Chemical Co. and used without further purification, was added to an aliquot (typically 500 μL) of purified blLAP solution. After overnight incubation at 4 °C, the blLAP–amastatin solution was passed through a Millex-GV filter. The initial blLAP–amastatin seed crystals were grown from this blLAP–amastatin solution at room temperature by hanging drop vapor diffusion against a crystallization buffer of 1:1 (v:v) 50 mM Tris/50 μM $ZnSO_4$/pH 7.8:2-methyl-2,4-pentanediol (MPD) (Jurnak et al., 1977). The MPD was purchased from Sigma Chemical Co. and used without further purification. Within 1 week, small hexagonal rod-like crystals approximately 0.1 mm in diameter and 0.3 mm in length appeared. One of these crystals was then removed to a 10-μL drop of MPD crystallization solution and allowed to reequilibrate at room temperature against a reservoir of 50 mM Tris/50 μM $ZnSO_4$/pH 7.8 by hanging drop vapor diffusion.

[2] The enzyme binding subsite designations S_i and S'_i, and the ligand residue designations P_i and P'_i, follow the convention of Schechter and Berger (1967).

Table I: Data Intensity Statistics by Resolution Shell

		cumulative percentages				
res (Å)	no. of refl	R_{merge}	$I \leq 1\sigma$	$I \leq 2\sigma$	$I \leq 3\sigma$	$I > 3\sigma$
8.90	490	0.036	0.4	1.4	3.7	96.3
6.44	786	0.052	1.3	2.8	5.3	94.7
5.30	994	0.073	0.7	3.3	5.7	94.3
4.61	1171	0.059	0.3	2.6	4.5	95.5
4.13	1320	0.062	0.5	2.3	4.5	95.5
3.78	1458	0.074	0.8	2.7	5.1	94.9
3.50	1570	0.087	0.8	2.7	5.4	94.6
3.28	1688	0.099	2.1	4.9	9.2	90.8
3.09	1797	0.111	2.3	7.0	13.1	86.9
2.93	1898	0.126	3.2	9.0	16.0	84.0
2.80	1959	0.137	3.4	10.9	20.8	79.2
2.68	2012	0.151	5.5	15.7	26.3	73.7
2.58	2064	0.165	6.9	20.0	33.6	66.4
2.48	2090	0.178	8.5	23.8	38.8	61.2
2.40	2019	0.183	12.0	29.1	45.4	54.6
overall	23316	0.089	4.0	11.2	19.0	81.0

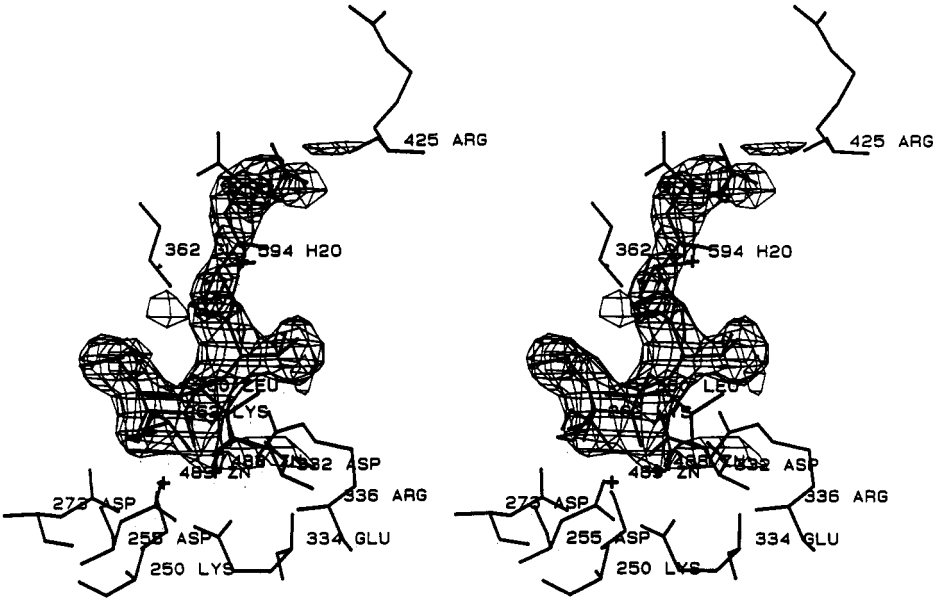

FIGURE 2: Stereoview of the $F_o - F_c$ map showing the electron density of amastatin bound in the active site of blLAP. The phases used in this map were calculated after refinement of the enzyme portion and prior to inclusion of amastatin in the model. The contour level of the map is 2.0σ. The final refined coordinates of Lys-250, Asp-255, Lys-262, Asp-273, Asp-332, Glu-334, Arg-336, Leu-360, Gly-362, Ala-363, Arg-425, Zn-488, Zn-489, Wat-594, and amastatin have been superimposed onto the map. The solvent cavity center of the blLAP hexamer is approximately to the upper right of this figure.

After 1 week, the seed crystal was removed to a 20-μL drop of fresh blLAP–amastatin solution and allowed to reequilibrate at room temperature by hanging drop vapor diffusion against a reservoir of MPD crystallization buffer. Within 2 weeks, the seed crystal would typically grow to a hexagonal rod 0.35 mm in diameter and 1.0 mm in length. Other small crystals which could subsequently be used as seeds would also appear in the seeded drop. This method of macroseeding to grow large blLAP–amastatin crystals could also be used to grow crystals of native blLAP which were consistently at least 0.35 mm in diameter and 1.0 mm in length. X-ray precession photographs taken at room temperature identified the space group of these blLAP–amastatin crystals as $P6_322$ with unit cell parameters a = 132.3 Å and c = 123.1 Å. There is one protomer of blLAP–amastatin complex in the asymmetric unit. This macroseeding method yielded large crystals of blLAP within 3–4 weeks of the preparation of a purified blLAP solution. X-ray diffraction studies were greatly facilitated by this crystallization method compared with the previous Li_2SO_4 crystallization method which required 1–3 months to grow blLAP crystals which on rare occasions were 0.25–0.3 mm in diameter (Burley et al., 1992).

X-ray diffraction data were collected at −150 °C on a Siemens X-100A multiwire area detector. Graphite monochromated Cu Kα radiation was produced by a Rigaku RU-200 rotating anode X-ray generator with a 500-μm focus cup operating at 50 kV and 150 mA. A Siemens LT-2 low-temperature apparatus was used to maintain the temperature. The blLAP–amastatin crystal was mounted in a wire loop free-standing thin film of the MPD crystallization solution (Teng, 1990). Solutions with high concentrations of MPD have previously been reported as good cryoprotective solvents (Petsko, 1975). Since the crystallization and cryoprotective buffers were the same for the blLAP–amastatin crystal, there was no danger of crystal damage due to osmotic shock in transferring the crystal from the hanging drops in which they grew onto the cryoprotective free-standing thin film. Under these conditions of data collection, the unit cell of the blLAP–amastatin crystal was determined by the data collection software BUDDHA (Blum et al., 1987) to be a = 130.3 Å and c = 121.9 Å. Such small changes in the unit cell parameters from those determined at room temperature are

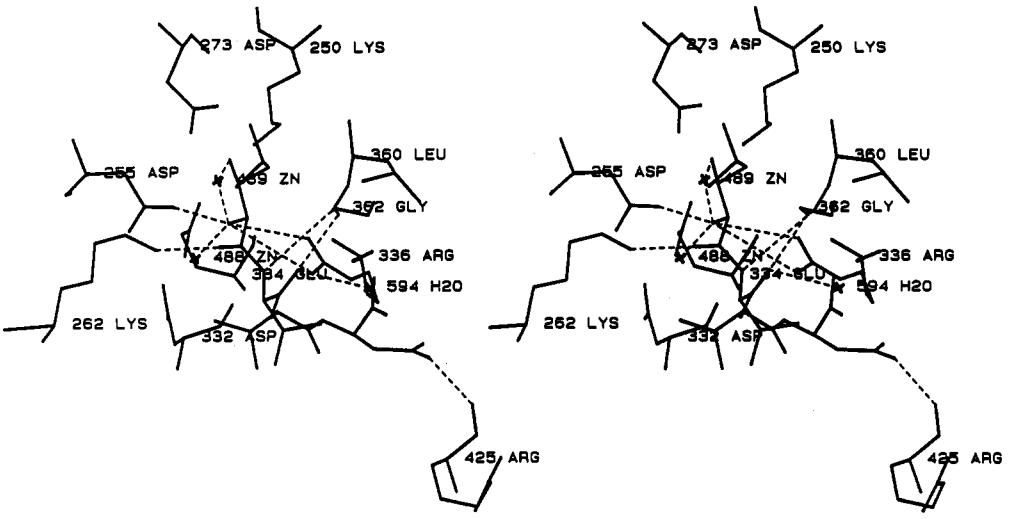

FIGURE 3: Stereoview of the active site of the blLAP–amastatin complex. This view is different from that of Figure 2. The solvent cavity center of the blLAP hexamer is approximately to the lower right of this figure. The enzyme–inhibitor interactions indicated by dashed lines are denoted by *a*'s in Table II.

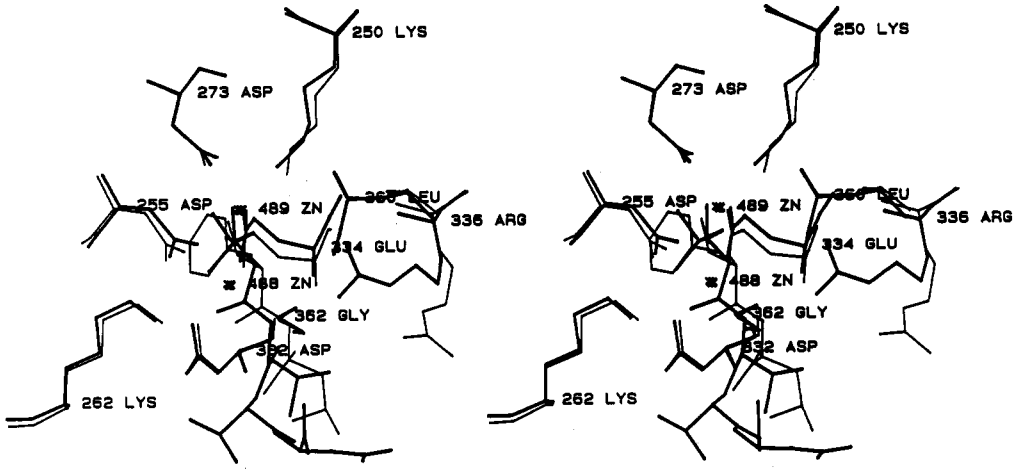

FIGURE 4: Stereoview of the active site of the blLAP–amastatin complex (thick lines) and the active site of the blLAP–bestatin complex (thin lines) after superposition of the C_α chain of the blLAP–amastatin complex onto the C_α chain of the blLAP–bestatin complex.

to be expected due to subtle changes in the packing of the protein with varying temperature (Tilton et al., 1992). Crystal decay due to radiation damage which hampers data collection at room temperature was practically absent under these low-temperature data collection conditions. A total of 940 area detector data frames were recorded from a single blLAP–amastatin crystal. The mean intensity of the reflections of the last 10 frames was only 6% lower than the mean intensity of the reflections of the first 10 frames. The complete data set includes 93 426 reflections between 30.0- and 2.4-Å resolution of which 23 316 reflections were unique (95% completeness). The merging R [$R_{merge} = \sum_{hkl}(\sum_i|I - \bar{I}|/\sum_i I)$] for all reflections was 0.089. The R_{merge} by resolution shell for the data is given in Table I. The 20 436 reflections between 10.0- and 2.4-Å resolution with intensity greater than 2σ were used in the refinement of the blLAP–amastatin structure.

The position of the blLAP–amastatin complex in the unit cell was determined by rigid body refinement using the 2.7-Å structure of native blLAP as the search model (Burley et al., 1990). The transformation relating the two structures involved essentially no rotation, and translations along the crystallographic x, y, and z axes of approximately 1, 0.4, and 0.7 Å, respectively. After rigid body refinement, the enzyme, without amastatin and waters, was refined by simulated annealing to a crystallographic residual [$R_{factor} = \sum_{hkl}(||F_o| - |F_c||/|F_o|)$] of 0.225. At this point, difference electron density maps ($F_o - F_c$) revealed amastatin bound in the active site (Figure 2). Amastatin and 132 waters were then built into the structure according to the difference electron density. Powell minimization and B-factor refinement of the entire structure resulted in a final structure with an R_{factor} of 0.198. All crystallographic refinements were executed by X-PLOR (Brünger et al., 1987; Brünger, 1990) on a Digital DECstation 3100. All model building was done on an Evans and Sutherland PS390 graphics system interfaced with a Digital VAXstation 3200 using the program FRODO (Jones, 1985).

RESULTS

The final refined structure of the blLAP–amastatin complex contains amino acid residues 1–11 and 15–484 and the two active site Zn^{2+}s of blLAP, the 33 non-hydrogen atoms of amastatin, and 132 waters. The deviations from ideal bond lengths and ideal bond angles are 0.015 Å and 3.4°, respectively. The expected uncertainty in coordinates is between 0.2 and 0.3 Å as indicated by a Luzatti plot (Luzatti, 1952; data not shown). Amino acid residues 12–14 and the three C-terminal residues 485–487 occur in solvent-exposed regions. Electron densities for these residues were not located in the previously reported structures of native blLAP and the

Table II: Selected blLAP–Amastatin Interactions

enzyme atom	inhibitor atom	distance (Å)
Zn-489 (site 2)	terminal amino N	2.1[a]
Lys-250 N_ζ	terminal amino N	3.2
Asp-255 $O_\delta1$	terminal amino N	3.1
Asp-273 $O_\delta1$	terminal amino N	3.0
Asp-273 $O_\delta2$	terminal amino N	2.4
Thr-359 carbonyl O	terminal amino N	2.9
Zn-488 (site 1)	P_1 hydroxyl O	2.1[a]
Zn-489 (site 2)	P_1 hydroxyl O	2.2[a]
Lys-250 N_ζ	P_1 hydroxyl O	4.0
Asp-255 $O_\delta1$	P_1 hydroxyl O	2.4[a]
Asp-332 $O_\delta2$	P_1 hydroxyl O	3.7
Asp-332 carbonyl O	P_1 hydroxyl O	3.2
Glu 334 $O_\epsilon1$	P_1 hydroxyl O	3.4
Glu-334 $O_\epsilon2$	P_1 hydroxyl O	3.6
Arg-336 $N_\eta1$	P_1 hydroxyl O	3.8[a]
Arg-336 $N_\eta2$	P_1 hydroxyl O	4.0[a]
Zn-488 (site 1)	P_1 carbonyl O	3.9
Asp-255 $O_\delta1$	P_1 carbonyl O	4.1
Lys-262 N_ζ	P_1 carbonyl O	2.7[a]
Asp-332 $O_\delta1$	P_1 carbonyl O	3.6
Asp-332 $O_\delta2$	P_1 carbonyl O	3.6
Zn-488 (site 1)	P'_1 amide N	4.0
Asp-332 carbonyl O	P'_1 amide N	3.2
Arg-336 $N_\eta1$	P'_1 amide N	3.4
Leu-360 carbonyl O	P'_1 amide N	3.9[a]
Gly-362 amide N	P'_1 carbonyl O	2.8[a]
Wat-594 O	P'_1 carbonyl O	2.8[a]
Wat-594 O	P'_2 carbonyl O	3.5
Wat-594 O	P'_3 amide N	3.8
Arg-425 carbonyl O	P'_3 carboxylate $O_\delta1$	3.3
Arg-425 carbonyl O	P'_3 carboxylate $O\delta_2$	2.4[a]
Gly-428 amide N	P'_3 carboxylate $O_\delta2$	3.7
Wat-594 O	P'_3 carboxylate $O_\delta2$	4.2
Gly-362 carbonyl O	terminal carboxylate O1	3.3
Ala-363 amide N	terminal carboxylate O1	3.1
Wat-594 O	terminal carboxylate O1	4.1

[a] These interactions are indicated by dashed lines in Figure 3.

blLAP–bestatin complex which were determined from X-ray diffraction data collected at room temperature (Burley et al., 1992). Electron densities for these residues were also absent in blLAP–amastatin electron density maps, although it was hoped that these regions would be stabilized enough to be located in maps calculated from X-ray diffraction data collected at −150 °C. Either these regions are intrinsically disordered or they are sufficiently disordered in the crystals at room temperature that flash-freezing the crystals at −150 °C may have stabilized multiple conformations of these residues. Since these six residues could not be located in any electron density maps, they were not included in the refinement of the blLAP–amastatin complex. The enzyme structure of the blLAP–amastatin complex is very similar to those of native blLAP and the blLAP–bestatin complex. Superposition of the blLAP–amastatin C_α chain onto the native blLAP C_α chain shows an rms deviation of 0.4 Å between the backbone atoms of the two structures. A similar comparison between the blLAP–amastatin complex and the blLAP–bestatin complex also results in an rms deviation of 0.4 Å.

One molecule of intact amastatin binds in the active site of blLAP (Figures 2 and 3). The binding mode of this tetrapeptide analogue inhibitor is similar to that of bestatin, a dipeptide analogue inhibitor (Burley et al., 1991, 1992; Kim et al., 1993) (Figure 4; Table II). For both inhibitors, Zn-489, the tightly bound site 2 metal, is coordinated by both the terminal amino nitrogen and the nonproteinaceous P_1 hydroxyl oxygen of the inhibitors. These two inhibitor functional groups of both amastatin and bestatin chelate the site 2 Zn^{2+} as was proposed by Takita (Nishizawa et al., 1977). The P_1 hydroxyl oxygen actually coordinates to both active site Zn^{2+}s as the two hydroxyl oxygen–Zn^{2+} distances are equal within experimental error for both blLAP–inhibitor complexes. Furthermore, the hydroxyl oxygen of amastatin also tends toward an interaction with the guanidinium group of Arg-336, whose side chain adopts two distinct conformations. One conformation of the Arg-336 side chain is directed more toward the active site than that seen in the 2.32-Å structure of native blLAP (Burley et al., 1992) (Figure 5). This conformation brings the guanidinium group of Arg-336 closer to the two active site Zn^{2+}s and the amastatin hydroxyl oxygen than does the other conformation, which resembles more that of the 2.32-Å structure of native blLAP. Completing the enzyme–inhibitor interactions involving the inhibitor P_1 portion in the blLAP–amastatin complex are the polar interaction between the P_1 carbonyl oxygen and the amino group of the Lys-262 side chain and the binding of the P_1 isobutyl side chain in the hydrophobic pocket formed by Thr-359, Met-270, Thr-361, and Leu-360. For the P'_1 portion of amastatin, hydrogen bonding interactions are seen between the amide nitrogen of amastatin and the backbone carbonyl oxygen of Leu-360 and between the carbonyl oxygen of amastatin and the amide nitrogen of Gly-362. The isopropyl side chain of the P'_1 valine residue of amastatin makes very little contact with the enzyme. The closest residues to this side chain are Asp-332 and Arg-336, which are respectively, 3.6 and 3.8 Å away.

Beyond the P'_1 portion, the bound amastatin is very near the solvent cavity at the center of the blLAP hexamer (Burley et al., 1990), and thus there are few enzyme–inhibitor interactions for the P'_2 and P'_3 portions of amastatin. Although the electron density corresponding to the P'_2 and P'_3 residues of amastatin is poorer than that for the P_1 and P'_1 residues, it is sufficient to establish unambiguously the direction of orientation of amastatin in the active site binding groove. The density is particularly weak at the P'_3 residue where no density is seen for the backbone terminal carboxylate, whose conformation was modeled to maximize hydrogen bonding interactions with the enzyme. Alternatively, the P'_3 residue can be modeled so that the terminal carboxylate fits into the electron density which is occupied by the side chain carboxylate, and the side chain carboxylate fits into the small bit of electron density in front of the C_α of this residue, toward the reader, in Figure 2. This alternative binding mode for the P'_3 residue is achieved primarily by a 120° rotation about the N–C_α bond of the P'_3 residue. Both carboxylates of the P'_3 residue fit into some electron density in this alternative binding mode, but there are no enzyme–inhibitor contacts for the side chain carboxylate. These two modes together reinforce the prominent electron density, while decreasing the density elsewhere. Since the P'_3 residue of amastatin is very near the surface of the blLAP protomer, it is likely that the binding of this residue is relatively disordered compared with the rest of the inhibitor. The conformation of the P'_3 residue depicted in Figures 2 and 3, and the alternative conformation of this residue, may be two of several conformations assumed by this residue in the blLAP–amastatin complex. The conformation of the P'_3 residue depicted in Figures 2 and 3 was chosen for the refinement of the structure of the blLAP–amastatin complex because this conformation showed the best fit into electron density for the side chain carboxylate and also allowed for the most enzyme–inhibitor interactions.

The Zn^{2+} coordination environments of the blLAP–amastatin structure, the blLAP–bestatin structure, and the native blLAP structure are similar (Figure 6). One small difference is the separation between the two Zn^{2+}s. The

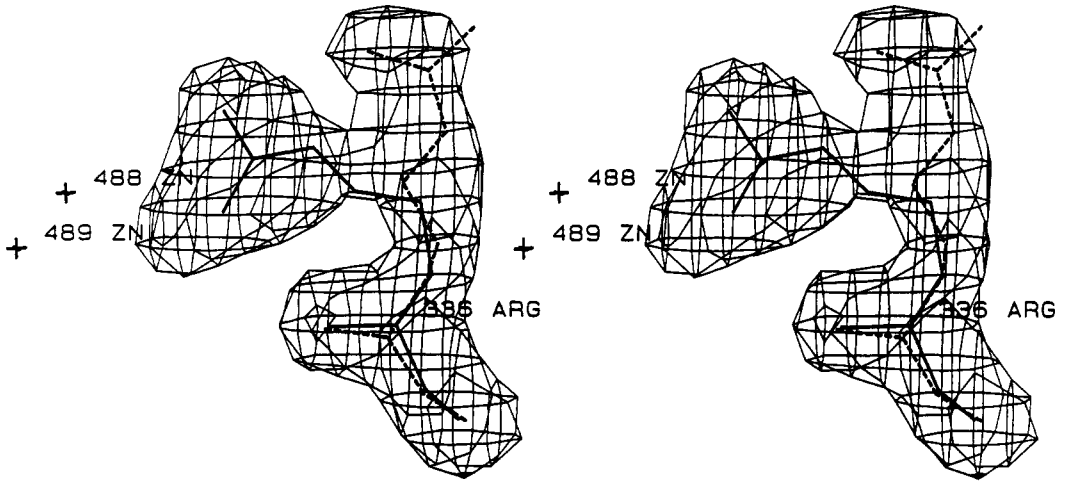

FIGURE 5: Stereoview of the $F_o - F_c$ electron density map calculated from the blLAP–amastatin data for which Arg-336 was omitted from the structure factor calculations showing the two conformations of Arg-336 in the blLAP–amastatin complex. The coordinates of the two refined conformations of Arg-336 and the active site Zn^{2+}s are superimposed onto the map. The conformation drawn in solid lines appears to be more catalytically productive than that drawn in dashed lines. The contour level for the map is 2.5σ.

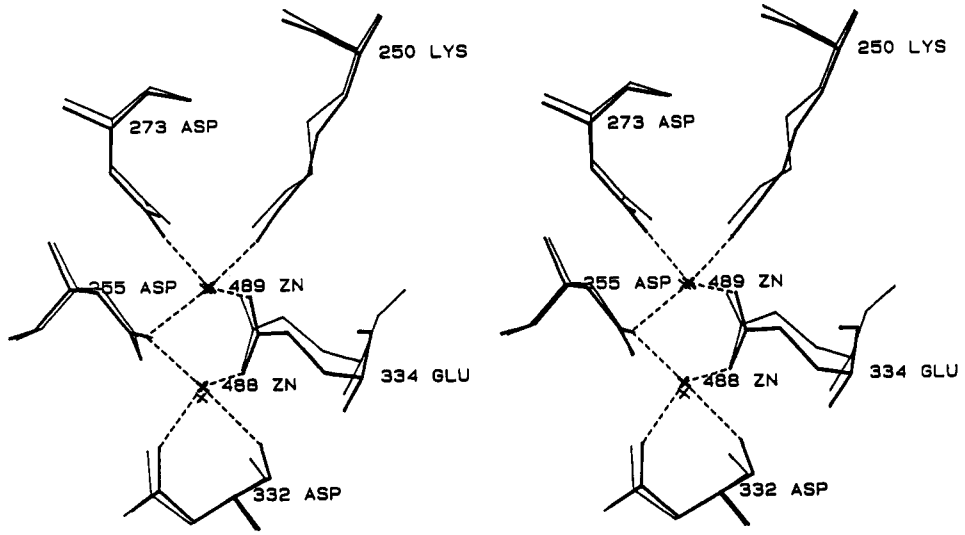

FIGURE 6: Stereoview of the active site Zn^{2+}s and the Zn^{2+} coordinating residues in the 2.32-Å structure of native blLAP (thick lines; Burley et al., 1992) and in the structure of the blLAP–amastatin complex (thin lines) after superposition of the C_α chain of the blLAP–amastatin complex onto the C_α chain of the 2.32-Å native blLAP structure.

distance between the two Zn^{2+}s increases slightly upon inhibitor binding. In native blLAP, the Zn^{2+}–Zn^{2+} separation is 2.9 Å. This distance increases to 3.1 and 3.3 Å, respectively, for the blLAP–bestatin (Burley et al., 1992; Kim et al., 1993) and the blLAP–amastatin complexes. This increased separation between the two Zn^{2+}s may be due to the coordination of both Zn^{2+}s by the P_1 hydroxyl oxygens of the inhibitors, perhaps driving the two Zn^{2+}s apart from each other. The increased separation between the two Zn^{2+}s in the blLAP–amastatin structure does not appear to be an effect of the low temperature at which the data were collected. The X-ray structure of native blLAP determined from data collected at low temperature (Kim & Lipscomb, 1993) shows the same 2.9-Å Zn^{2+}–Zn^{2+} separation as does the structure of native blLAP which was determined from data collected at ambient temperature (Burley et al., 1992). In spite of the slight differences in Zn^{2+}–Zn^{2+} separation, the Zn^{2+} coordination by enzymic amino acid residues is conserved among all blLAP X-ray structures.

DISCUSSION

Amastatin Binding Mode. The binding mode of amastatin in the active site of blLAP is very similar to that of bestatin (Burley et al., 1991, 1992; Kim et al., 1993) (Figure 4). Most notable is that these two inhibitors exhibit the same N-terminus-to-C-terminus orientation in the active site binding groove. Amastatin and bestatin are slow-binding inhibitors of LAP (Wilkes & Prescott, 1985). It had previously been speculated that the step responsible for slow-binding inhibition by bestatin involved the reversal of initial binding about its C2 scissile bond analogue in the S_1 and S'_1 subsites. A reversal of binding step is conceivable for bestatin because bestatin is a dipeptide analogue inhibitor. Since blLAP is an aminoexopeptidase, it can be reasonably assumed that the active site binding groove is asymmetric, lacking an S_2 binding subsite (Harbeson & Rich, 1988). Sterically, the N-terminal binding pocket of blLAP can accommodate either the N-terminal or C-terminal residue of a dipeptide analogue inhibitor binding in either a true or reversed N-terminus-to-C-terminus orientation. A longer peptide analogue inhibitor would preclude any nonspecific reversal of binding about the scissile bond analogue if it is assumed that the "dead end" N-terminal pocket of the blLAP active site binding groove accommodates only one ligand residue. Since the binding mode of amastatin, a tetrapeptide analogue, shows the same N-terminus-to-C-terminus orientation as that of bestatin, the slow binding of

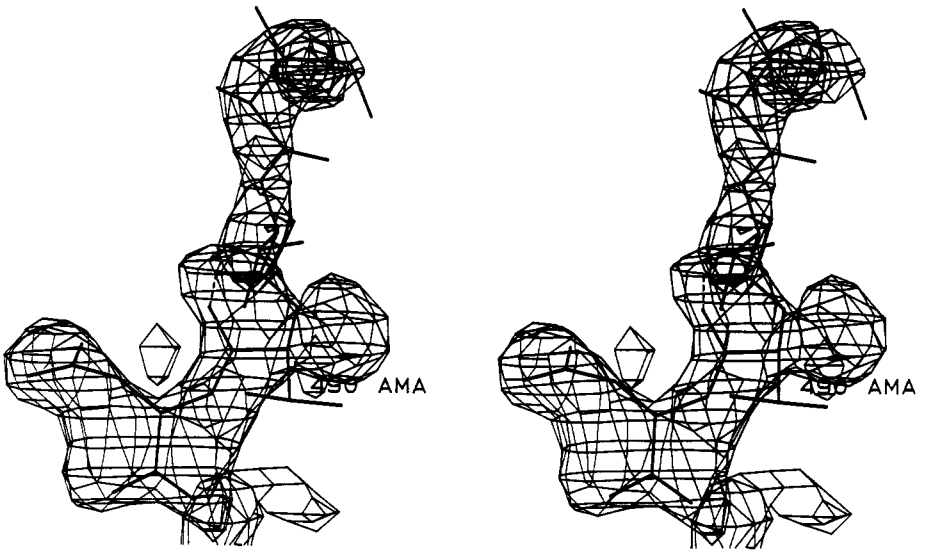

FIGURE 7: Stereoview of the modeled fit of amastatin in a reversed N-terminus-to-C-terminus orientation with respect to the orientation of amastatin in Figures 2 and 3. The electron density is from the $F_o - F_c$ map depicted in Figure 2. The valine side chain of the P'_2 residue is labeled, and the unfavorable (1.6 Å) interaction between the P'_1 and P'_2 carbonyl oxygens is indicated by dashed lines.

amastatin and bestatin is likely not due to a reversal of binding about the scissile bond analogues of these inhibitors which results in the binding modes seen in the structures of these blLAP–inhibitor complexes. It had also been previously speculated that bestatin, again because of its dipeptide nature, was binding to blLAP nonspecifically in an N-terminus-to-C-terminus orientation opposite to that of a true peptide substrate (David, 1991). Since the N-terminus-to-C-terminus orientation of the binding modes of bestatin and amastatin are the same, this backbone orientation likely also applies to peptide substrates of blLAP.

The possibility that amastatin was binding to blLAP in a nonspecific reversed binding mode about the midpoint of its backbone, and not about its C2 scissile bond analogue, was also considered. The relative steric symmetry of the side chains of amastatin, Leu-Val-Val-Asp, raised the possibility that it was incorrectly modeled into its electron density. Amastatin was thus remodeled into the difference electron density in the active site of blLAP in an N-terminus-to-C-terminus orientation which is opposite to that depicted in Figure 2 (Figure 7). Although the backbone of amastatin in this reversed binding mode fits reasonably well into the electron density, the P'_2 valine residue of amastatin is severely mismodeled, as indicated by the failure of the side chain of this residue to fit the electron density. In addition, there are some unfavorable molecular conformations in amastatin in this reversed binding mode. The peptide bond linking the P'_2 and the P'_3 residues of amastatin deviates 50° from the energetically favorable planar *trans* conformation. This modeling also places the carbonyl oxygens of the P'_1 and the P'_2 residues only 1.6 Å from each other. Furthermore, in this reversed binding mode, the specificity of the S_1 subsite of LAP for amino acid residues with hydrophobic side chains (Smith & Spackman, 1955) would be violated since this subsite would be occupied by the aspartic acid of amastatin. The N-terminus-to-C-terminus orientation depicted in Figure 2 is clearly correct for blLAP-bound amastatin.[3]

The positions of the two active site Zn^{2+}s and the N-terminus-to-C-terminus orientation of binding of amastatin and bestatin may account for some aspects of the slow binding of these inhibitors. The active site binding groove is located in the blLAP protomer such that, in the blLAP hexamer, the

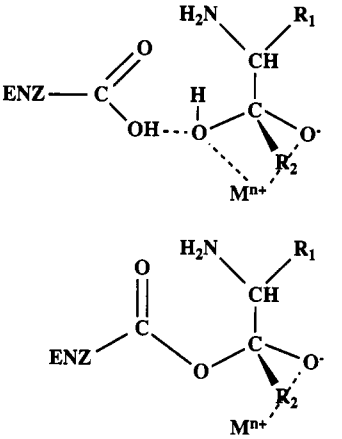

FIGURE 8: (Top) Transition state intermediate in the general base mechanism for proteolysis by a metalloaminopeptidase. The general base is depicted as a carboxylate-bearing residue which has abstracted a proton from the nucleophilic water. (Bottom) Transition state intermediate in the anhydride mechanism for proteolysis by a metalloaminopeptidase. The scissile carbonyl attacking species is depicted as a carboxylate-bearing residue. ENZ = enzyme. Covalent bonds are drawn as solid lines, and hydrogen bonds are drawn as dashed lines.

six active site binding grooves line the solvent cavity interior of the hexamer (Burley et al., 1990). Relative to the solvent cavity, the site 2 Zn^{2+} is deeper in the active site binding groove than is the site 1 Zn^{2+}. The crystallographically determined binding modes of amastatin and bestatin indicate that these inhibitors most likely enter the active site binding groove N-terminus first. As these inhibitors enter the active site binding groove, they would encounter the site 1 Zn^{2+} before the site 2 Zn^{2+}. It may be that these inhibitors coordinate the site 1 Zn^{2+} before they settle into their crystallographically determined binding modes in which they coordinate the site 2 Zn^{2+}. A slow step in binding would then entail dissociation from the site 1 Zn^{2+} and subsequent

[3] By these X-ray crystal structures, we cannot, however, exclude an early step in the binding of amastatin and bestatin in which these inhibitors are bound in the N-terminus-to-C-terminus orientation opposite to that depicted in Figure 2. In such an N-terminus-to-C-terminus orientation, the inhibitors bind to one or both Zn^{2+}s by their C-terminal carboxylates, or by the P'_3 side chain carboxylate of amastatin (Figure 7), and subsequently reverse in order to increase the enzyme–inhibitor interactions.

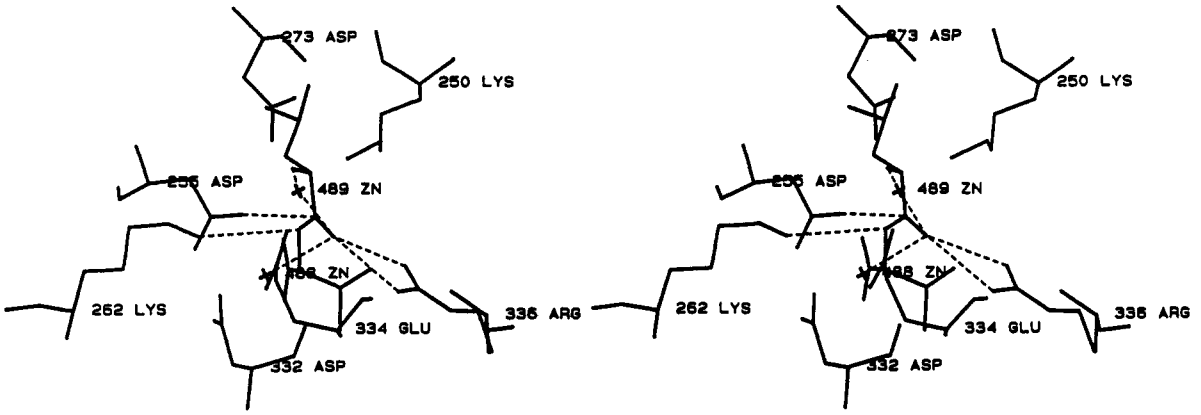

FIGURE 9: Stereoview of the substrate L-leucyl-L-valine (LV) modeled into the active site of blLAP. The coordinates of Lys-250, Asp-255, Asp-273, Lys-262, Asp-332, Glu-334, Arg-336, Zn-488, Zn-489, and LV are shown. The interactions indicated by dashed lines are denoted by *a*'s in Table III. This is LV binding mode I as described in the text.

coordination to the site 2 Zn^{2+}. Previously, Rich had proposed a mechanism for the slow binding of amastatin and bestatin which invoked two enzyme–inhibitor species, a collision complex followed by a tightened complex (Rich et al., 1984). From the structures of the blLAP–amastatin and blLAP–bestatin complexes, it is plausible that the site 1 metal-bound inhibitor is the collision complex and the site 2 metal-bound inhibitor is the tightened complex. A recent study on bestatin inhibition of blLAP determined that the dissociation constants of the "initial" and "final" blLAP–bestatin complexes are approximately 1.1×10^{-7} and 1.3×10^{-9} M, respectively (Taylor et al., 1993). These dissociation constants may correspond to the site 1 metal- and site 2 metal-bound inhibitor complexes proposed herein. This type of "metal relay" binding mechanism may also account for the two intermediates detected in the proteolysis of a C-terminal dansyl modified dipeptide substrate by pkLAP at low-temperature nonturnover conditions (Van Wart & Lin, 1983; Lin et al., 1988b). If a peptide substrate enters the active site binding groove of blLAP N-terminus first, its terminal amino nitrogen, and possibly also its scissile carbonyl oxygen, could sequentially coordinate to the two active site Zn^{2+}s as amastatin and bestatin are proposed to do. It is possible to model two binding modes for the dipeptide substrate L-leucyl-L-valine (LV) in the active site binding groove of blLAP in which the terminal amino and the scissile carbonyl of LV coordinate to Zn-488 in one binding mode, and to Zn-489 in the other. Consistent with this binding mechanism, only a single pre-steady-state intermediate was detected in proteolysis of a dansyl dipeptide substrate by site 1-unoccupied pkLAP under conditions which revealed two intermediates in proteolysis by di-metal pkLAP (Lin et al., 1988b). This result would be expected by this "metal relay" binding mechanism, since the ligand would bypass the unoccupied metal binding site 1 and bind directly to the site 2 metal.

Mechanism of Catalysis. Although there is much that remains unknown about the mechanism of LAP catalysis, most of the studies of LAP thus far, including the X-ray structural determinations of blLAP, tend to implicate a general base mechanism for catalysis. In such a mechanism, the scissile carbonyl of the intact substrate is attacked by an active site water. A water can be activated to a more nucleophilic hydroxide-like state by its interactions with metals and amino acid residues acting as general bases. The transition state in such a general base mechanism is a tetrahedral *gem*-diolate, and there are no covalent bonds between amino acid residues of the enzyme and reaction intermediate species during catalysis (Figure 8). Amastatin and bestatin have generally been assumed to behave as transition-state analogues in their binding to LAP (Nishizawa et al., 1977; Nishino & Powers, 1979; Ricci et al., 1982; Harbeson & Rich, 1988). The tetrahedral sp^3-hybridized hydroxyl-bearing C2 carbon is thought to mimic the tetrahedral hydrated scissile carbonyl in a general base mechanism. Another widely suggested catalytic mechanism for peptidases is the anhydride pathway in which the scissile carbonyl of the substrate is attacked directly by a nucleophilic enzymic residue. Such an attack results in a covalent acyl enzyme–ligand intermediate as in proteolysis of certain substrates by serine proteases (Sweet et al., 1974; Blow, 1976). The structures of native blLAP and its complexes with amastatin and bestatin do not show any nucleophilic amino acid residues in the active site which are in a position to execute direct nucleophilic attack on the scissile carbonyl of a substrate, assuming that the C2 of amastatin and bestatin are the analogues of the scissile carbonyl carbon in a true peptide substrate. An anhydride mechanism for catalysis appears to be unlikely for blLAP due to the arrangement of its active site residues.

In order to develop a catalytic mechanism for blLAP in which the transition state could be mimicked by the binding mode of amastatin, the dipeptide substrate L-leucyl-L-valine (LV) and its putative *gem*-diolate transition state (LVTS) were modeled into the active site of blLAP based on the structure of blLAP-bound amastatin (Figures 9 and 10). LV was chosen as the substrate model since the P_1 and P'_1 residues of amastatin are leucine-like and valine, respectively. Initially, LV was modeled into the active site of blLAP so that the bonds flanking its scissile carbonyl were maximally superimposed onto C1–C2–C3 of amastatin while the enzyme portion of the blLAP–amastatin complex was left unchanged. This preliminary modeled binding mode resulted in unacceptably close contacts between the P'_1 valine side chain of LV and the side chain of Arg-336. Such an unfavorable interaction is not seen in the blLAP–amastatin complex due to the nonproteinaceous C2 of amastatin which effectively displaces the atoms to its C-terminus side away from the Arg-336 side chain and toward the solvent cavity center of the blLAP hexamer. To alleviate unreasonably close contacts with the enzyme, LV was raised ~0.5 Å from the active site Zn^{2+}s and Arg-336, resulting in the final modeled binding mode of LV in the active site of blLAP, LV binding mode I (Figure 9; Table III).

No proposal for a catalytic mechanism for LAP can be complete without roles for the active site metals, both of which have been shown to affect catalysis by blLAP (Allen et al., 1983). Metal-free apo-blLAP has no enzymatic activity

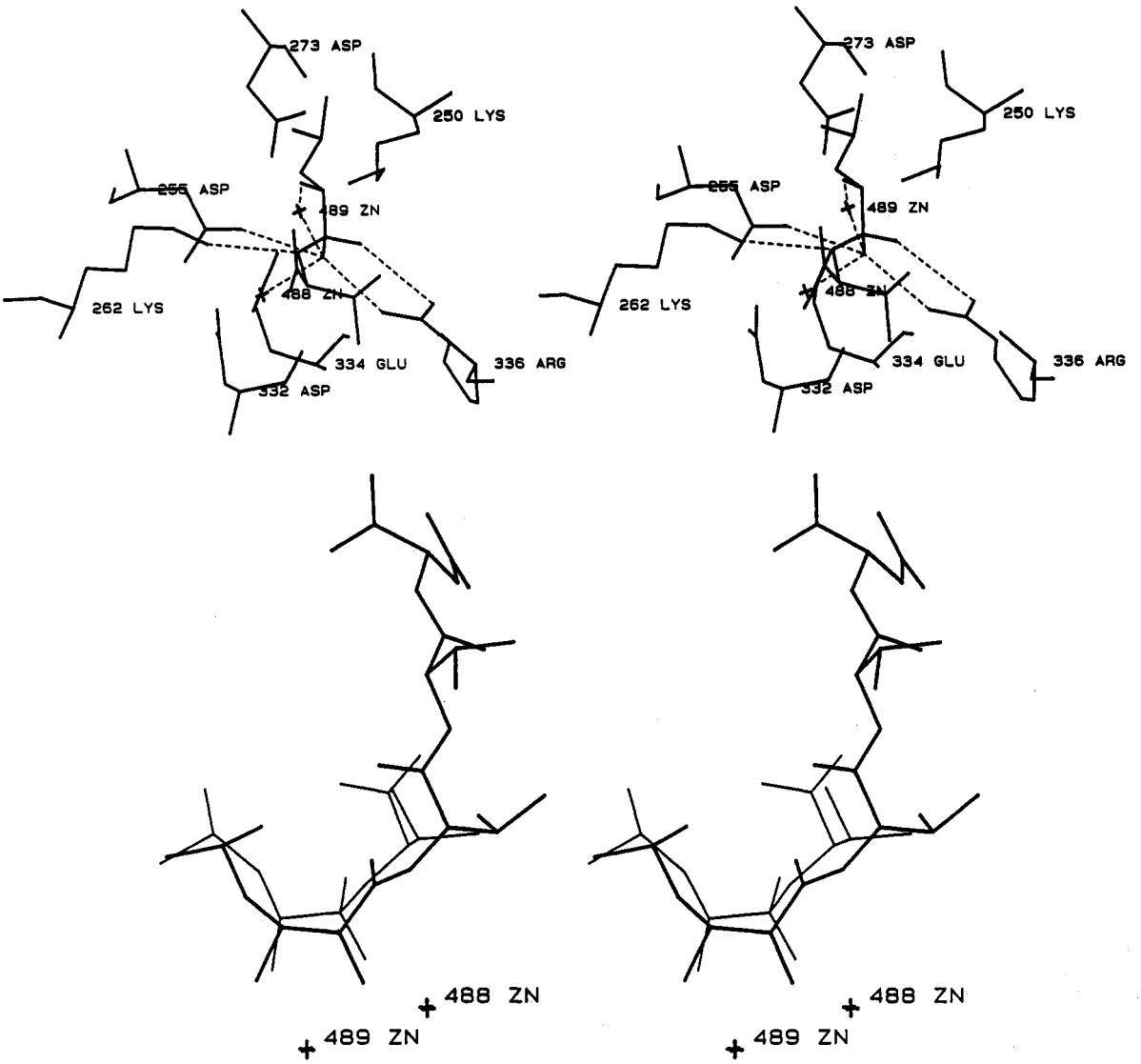

FIGURE 10: (Top) Stereoview of the putative *gem*-diolate transition state of L-leucyl-L-valine (LVTS) modeled into the active site of blLAP. The coordinates of Lys-250, Asp-255, Lys-262, Asp-273, Asp-332, Glu-334, Arg-336, Zn-488, Zn-489, and LVTS are shown. The interactions indicated by dashed lines are denoted by *a*'s in Table IV. O_a of the *gem*-diolate is to the right of O_b in this view. (Bottom) Stereoview of the modeled LVTS binding mode (thin lines) superimposed onto the crystallographically determined binding mode of amastatin (thick lines). O_a of the *gem*-diolate of LVTS is above O_b in this view. The coordinates of the Zn^{2+}s from the blLAP–amastatin complex are also shown.

Table III: Selected blLAP–LV Interactions

enzyme atom	substrate atom	distance (Å)
Zn-488 (site 1)	terminal amino N	3.9
Zn-489 (site 2)	terminal amino N	2.1[a]
Lys-250 N_ζ	terminal amino N	3.6
Asp-255 $O_\delta1$ O	terminal amino N	2.6
Asp-273 $O_\delta1$	terminal amino N	3.1
Asp-273 $O_\delta2$	terminal amino N	2.8
Asp-255 $O_\delta1$	scissile carbonyl C	3.5[a]
Zn-488 (site 1)	scissile carbonyl O	2.9[a]
Zn-489 (site 2)	scissile carbonyl O	3.2[a]
Asp-255 $O_\delta1$	scissile carbonyl O	3.5
Asp-332 carbonyl O	scissile carbonyl O	3.2
Arg-336 $N_\eta1$	scissile carbonyl O	3.1[a]
Arg-336 $N_\eta2$	scissile carbonyl O	3.9[a]
Leu-360 carbonyl O	scissile carbonyl O	3.2
Lys-262 N_ζ	P'_1 amide N	3.3

[a] These interactions are indicated by dashed lines in Figure 9.

(Hanson & Frohne, 1976). The crystallographically determined binding modes of amastatin and bestatin, and the modeled binding mode of LV, show that the N-terminal nitrogens of these ligands are coordinated to Zn-489, the tightly bound site 2 metal. For the closely related pkLAP, it has been shown that although the enzyme has two metal binding sites, the site 1 metal is not necessary for catalysis (Himmelhoch, 1969; Shen & Melius, 1977; Van Wart & Lin, 1981). This result may also apply to blLAP, although we are unaware of any reports of kinetic studies of single-metal blLAP. It appears that one aspect of the absolute requirement of the site 2 metal in LAP catalysis is its role in substrate binding *via* the N-terminal amine nitrogen of the substrate. A poor N-terminal amine–site 2 Zn^{2+} interaction may account for the observation that N-blocked species are not hydrolyzed by pkLAP while their corresponding compounds with free N-termini are hydrolyzed by pkLAP (Smith & Spackman, 1955). The proximity of the N-terminal amine nitrogens of amastatin and bestatin to the site 2 Zn^{2+}, 2.1 and 2.3 Å, respectively, indicates that the N-terminal amines of these bound inhibitors are most likely in their neutral, unprotonated forms. The pH dependencies of inhibition and kinetic parameters for the inhibitor L-leucinal and the substrate leucine-*p*-nitroanilide show inflections near pH 8, which is near the terminal amino pK_a values in solution for these compounds (Andersson et al., 1985). Although this pH result presumably reflects that the terminal amine of a ligand should be in its

unprotonated form for binding to occur, this presumption is not proven by this pH result since the indicated pH could be associated with the ionization of an enzymic amino acid residue or a metal-bound water.

The active site Zn^{2+}s are also involved in binding the hydroxyl oxygens of amastatin and bestatin and also the scissile carbonyl oxygen of LV. Due to the *S* configuration of the C2 of amastatin, the hydroxyl oxygen of amastatin points toward the Zn^{2+}s while the oxygen of the planar scissile carbonyl group of LV in its modeled binding mode points away from the Zn^{2+}s. The orientation of the scissile carbonyl of LV consequently places the scissile carbonyl oxygen of LV within hydrogen bonding distance of the guanidinium group of Arg-336, in addition to its interactions with the Zn^{2+}s (Table III). Such an interaction between the ligand and Arg-336 is much weaker in the blLAP–amastatin complex as the hydroxyl oxygen points away from Arg-336 and is 3.8 and 4.0 Å from its guanidinium nitrogens (Table II). This interaction appears to indicate a role for Arg-336 in binding and activating the substrate during catalysis.

$F_o - F_c$ electron density maps in which Arg-336 was omitted from the structure factor calculations revealed that the side chain of Arg-336 assumes two distinct conformations in the blLAP–amastatin complex (Figure 5). One conformation brings the guanidinium group of this residue much closer to the active site Zn^{2+}s and the amastatin hydroxyl oxygen than does the other conformation. The blLAP–amastatin structure was refined with the side chain of Arg-336 in the conformation closer to the two Zn^{2+}s and the amastatin hydroxyl oxygen since this conformation of the Arg-336 side chain appeared to be more catalytically productive than the alternative conformation. The alternative conformation of the Arg-336 side chain, whose electron density appears to be slightly weaker, resembles more that of the 2.32-Å structure of native blLAP. The side chain of Arg-336 was rebuilt to fit this alternative density and the enzyme-only portion of the blLAP–amastatin complex was rerefined by simulated annealing. The resulting structure was identical to the enzyme portion of the blLAP–amastatin structure shown in Figures 2 and 3, save for the conformation of the Arg-336 side chain. The multiple conformations of the Arg-336 side chain and the model of the blLAP–LV complex appear to indicate that the side chain of Arg-336 can move upon substrate binding to interact with and polarize the scissile carbonyl, thereby promoting nucleophilic attack. Such an electrophilic role may be shared with Zn-488, the readily exchangeable site 1 Zn^{2+}, which also interacts with the scissile carbonyl oxygen of LV. The presence of Arg-336 may preclude the absolute requirement of the site 1 metal in catalysis, as in the case of native pkLAP (Van Wart & Lin, 1981). Arg-336 is found in the amino acid sequence of the *pepA*-encoded aminopeptidases from *E. coli* and *S. typhimurium*, so it may be conserved in other aminoexopeptidases as well (Stirling et al., 1988, 1989). A similar electrophilic role for an active site arginine and an active site histidine has previously been proposed for the mechanisms of carboxypeptidase A and thermolysin, respectively (Matthews, 1988; Christianson & Lipscomb, 1989; Kim & Lipscomb, 1991).

The putative *gem*-diolate transition state of LV (LVTS) was then modeled into the active site of blLAP by transforming the trigonal planar sp^2-hybridized scissile carbonyl group of LV into the tetrahedral sp^3-hybridized *gem*-diolate group of LVTS which would result from the nucleophilic attack of a water on the scissile carbonyl carbon of LV (Figure 10; Table IV). As depicted in Figure 9, the modeled binding mode of LV necessitates that the nucleophilic attack by a water on the scissile carbonyl carbon of LV comes from the left side of the active site due to the orientation of the LV carbonyl group. A water executing a nucleophilic attack from this side of the active site binding groove could be activated by one or both of the Zn^{2+}s. The pK_as of Zn^{2+}-bound waters in model systems intended to mimic proteolysis have been measured to be as low as 7 (Groves & Olson, 1985). In addition, Asp-255, *via* its side chain carboxylate oxygen $O_\delta 1$, is in position to act as a possible general base in catalysis. $O_\delta 1$ of Asp-255 is 3.5 Å from the scissile carbonyl carbon of LV in the blLAP–LV model (Figure 9; Table III). This oxygen is also within interaction distance of both active site Zn^{2+}s (Figure 6). The coordination geometry of its side chain carboxylate group indicates that Asp-255 is probably much more involved in coordinating Zn-488 than Zn-489. Zn-488 is *syn* to the carboxylate and within the plane of the carboxylate, whereas Zn-489 is *anti* to the carboxylate and more than 1.0 Å out of the plane of the carboxylate (Kim & Lipscomb, 1993). The Zn-488 binding role of Asp-255 may seem to preclude this residue from additional catalytic roles since such roles would likely require a disruption of the $O_\delta 1$–Zn-488 interaction. However, the other side chain carboxylate oxygen of Asp-255, $O_\delta 2$, is in position to interact with Zn-488. In the blLAP–amastatin structure, the $O_\delta 2$–Zn-488 distance is 2.9 Å. It may be that Asp-255 acts as a general base upon a conformational change in its carboxylate side chain which frees $O_\delta 1$ from its Zn-488 binding role and allows it to abstract a proton from an active site water. Concomitantly, $O_\delta 2$ of Asp-255 may be brought into position to bind Zn-488, thus preserving the coordination number of this metal during catalysis.

The *gem*-diolate of LVTS would bear a formal negative charge on the oxygen which was once the carbonyl oxygen of LV. This *gem*-diolate oxygen of LVTS arising from the scissile carbonyl oxygen of LV will be referred to as O_a. As previously suggested, a negatively charged tetrahedral *gem*-diolate species occurring in blLAP catalysis could be stabilized by several components of the enzyme (Burley et al., 1991) (Figure 11). Both Zn^{2+}s are in position to stabilize the *gem*-diolate *via* interactions with the lone pair electrons of the oxygen which was once the nucleophilic water. This *gem*-diolate oxygen of LVTS will be referred to as O_b. In addition to the Zn^{2+}s, LVTS can be stabilized by the side chain of Arg-336, which can be modeled to assume a conformation allowing more favorable interactions between its guanidinium group and the *gem*-diolate oxygens. This conformation of the Arg-336 side chain is different from the two conformations seen in the

Table IV: Selected blLAP–LVTS Interactions

enzyme atom	transition state atom	distance (Å)
Zn-488 (site 1)	terminal amino N	3.9
Zn-489 (site 2)	terminal amino N	2.2[a]
Lys-250 N_ζ	terminal amino N	3.7
Asp-255 $O_\delta 1$ O	terminal amino N	2.6
Asp-273 $O_\delta 1$	terminal amino N	3.1
Asp-273 $O_\delta 2$	terminal amino N	2.8
Arg-336 $N_\eta 2$	*gem*-diolate O_a	3.6[a]
Leu-360 backbone carbonyl O	*gem*-diolate O_a	3.0
Zn-488 (site 1)	*gem*-diolate O_b	2.4[a]
Zn-489 (site 2)	*gem*-diolate O_b	2.7[a]
Asp-255 $O_\delta 1$	*gem*-diolate O_b	2.9[a]
Asp-332 carbonyl O	*gem*-diolate O_b	3.1
Arg-336 $N_\eta 1$	*gem*-diolate O_b	3.2[a]
Arg-336 $N_\eta 2$	*gem*-dillate O_b	4.0
Lys-262 N_ζ	P'_1 amide N	2.9[a]

[a] These interactions are indicated by dashed lines in Figure 10.

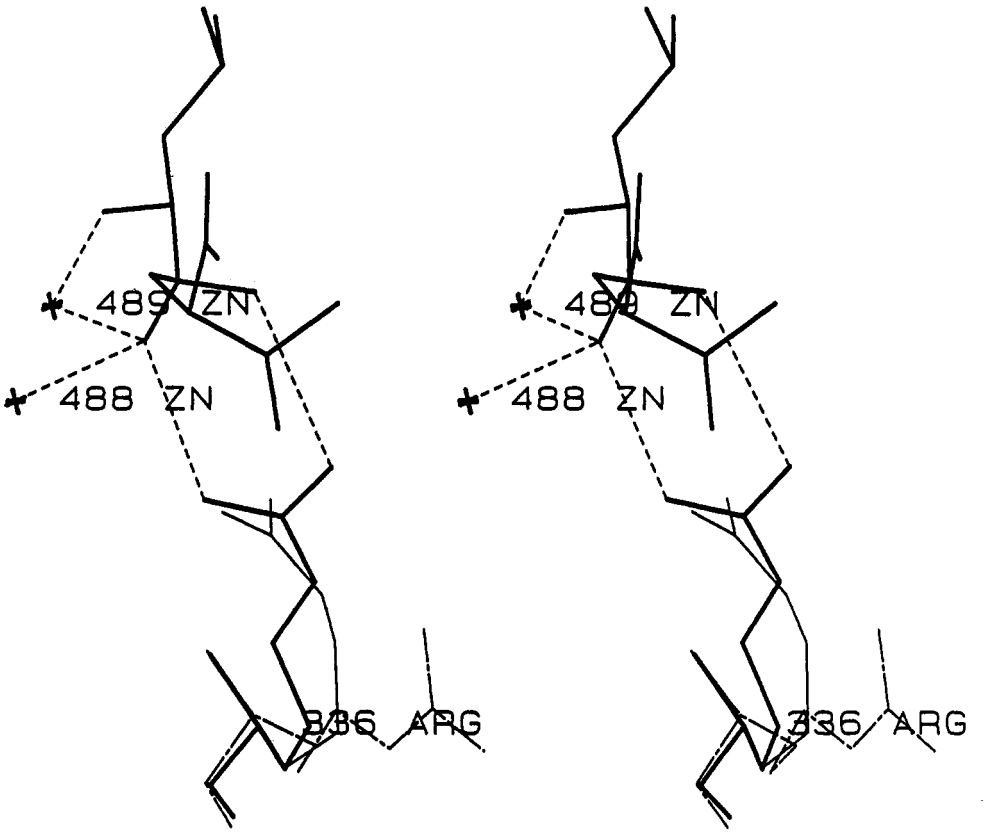

FIGURE 11: Stereoview of the modeled stabilization of the *gem*-diolate group of LVTS by the Zn^{2+}s and Arg-336 in blLAP (thick lines). As explained in the text, this model of transition state stabilization requires a conformational change in the side chain of Arg-336 from those seen in the crystallographically determined structure of the blLAP–amastatin complex. The two conformations of the Arg-336 side chain in the blLAP–amastatin complex are also shown (thin lines, broken lines). *gem*-Diolate oxygen O_a is to the right of *gem*-diolate oxygen O_b in this view.

blLAP–amastatin structure (Figure 11). In this conformation, the guanidinium group of Arg-336 and the *gem*-diolate group of LVTS are approximately coplanar, allowing both N_η nitrogens of Arg-336 to interact with both *gem*-diolate oxygens of LVTS in a salt link. The interaction of *gem*-diolate O_b of LVTS with this conformation of the Arg-336 side chain may also represent a binding site for a nucleophilic water which develops during catalysis with such subtle conformational changes in the enzyme (Kim & Lipscomb, 1993). Decomposition of LVTS to products would be facilitated by an active site proton donor to the P'_1 backbone nitrogen of LVTS, which would make the incipient C-terminal product a better leaving group. Lys-262 appears to be a likely candidate for this proton shuttling role. Its interactions with the P_1 carbonyl of amastatin in the crystallographically determined blLAP–amastatin complex and the P'_1 backbone nitrogen of LVTS in the modeled blLAP–LVTS complex indicate that its side chain amino group is in a position to provide a proton to the product leaving group (Figures 3 and 10; Tables II and IV). A schematic representation of the current X-ray structure-based mechanism for blLAP is depicted in Figure 12. Because a possible nucleophilic active site water has not been located in any blLAP structures, it is unknown which, or both, of the Zn^{2+}s activates the water for its proposed attack on the substrate. Zn-489, the site 2 metal, may be more involved in such a crucial activation of a water than Zn-488, the site 1 metal, is since pkLAP is active even when site 1 is unoccupied[4] (Van Wart & Lin, 1981). The proposed mechanism assumes that the nucleophilic water is activated predominantly by Zn-489.

Although the proposed mechanism is plausible and consistent with the structure of the blLAP active site, it is certainly not proven. One of the difficulties in formulating a mechanism for blLAP catalysis is that no catalytically important enzymic amino acid residues have yet been identified by biochemical methods, such as site-directed mutagenesis. The enzymic amino acid residues featured in the proposed mechanism have been identified by their crystallographically determined interactions with amastatin and bestatin. In spite of the dearth of more concrete biochemical studies detailing the mechanism of blLAP catalysis, the mechanism proposed in Figure 12 is compatible with some previous biochemical results. The pH profile of blLAP activity with respect to the substrate L-leucineamide indicates activity between pH 6 and 11 with a single maximum at pH 9 (Melbye & Carpenter, 1971). This pH profile is compatible with the roles proposed for Asp-255 and Arg-336. At pH 9, the carboxylate group of Asp-255, with a pK_a of ~4, would be in its unprotonated form, consistent with its proposed role as a general base. Also at this pH, the guanidinium group of Arg-336, with a pK_a of ~13, would be in its protonated formally monocationic state as depicted *in*

[4] An intriguing possibility is that the binding of substrates to single-metal "native" pkLAP creates a binding site for a second divalent metal. A certain substrate analogue inhibitor of porcine kidney fructose-1,6-bisphosphatase binds in the active site of this enzyme with either two Zn^{2+}s or two Mn^{2+}s, but, at the same metal concentrations, a different ligand binds with only one metal (Zhang et al., 1993). For pkLAP, it may be that, *in vivo*, the concentrations of free divalent metals are sufficiently high [~400 μM total Zn^{2+} in pig kidney (Wagstaffe et al., 1979; Long, 1961)] to allow the binding of a second metal upon substrate binding. Alternatively, the *in vivo* metal concentrations may be sufficiently high to keep both metal binding sites in pkLAP continually occupied, in contrast with the controlled metal concentrations of the *in vitro* studies of metal-substituted pkLAP (Van Wart & Lin, 1981; Lin et al., 1988a).

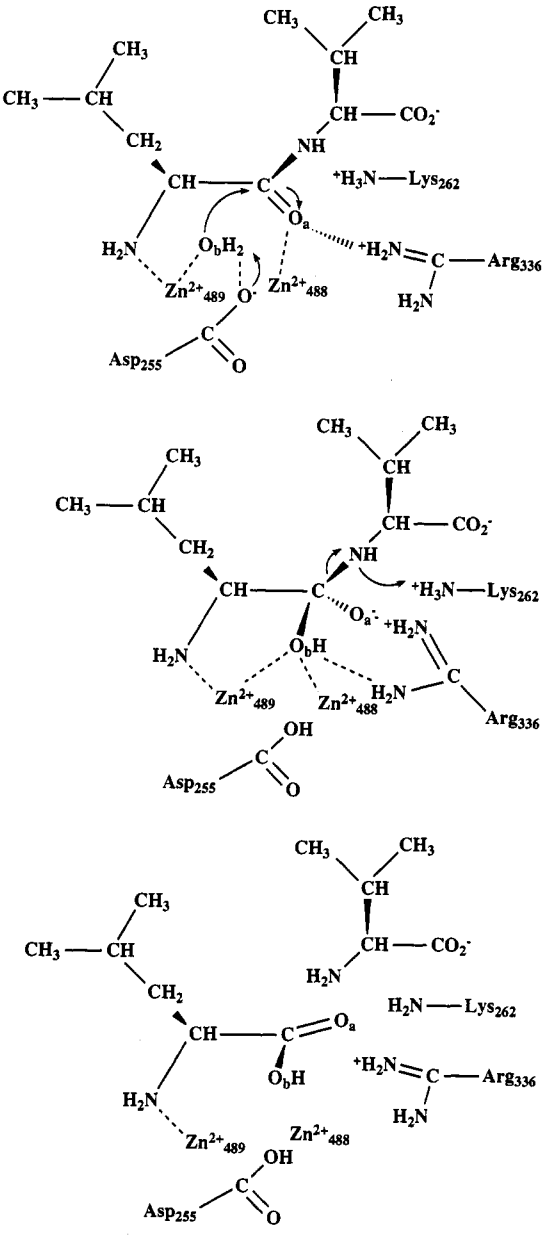

FIGURE 12: Proposal for the mechanism of blLAP catalysis. Covalent bonds are drawn as solid lines and noncovalent bonds are drawn as dashed lines. (a) The substrate L-leucyl-L-valine (LV) is bound to the site 2 Zn^{2+} (Zn-489) in the active site *via* its terminal amino nitrogen. A site 2 Zn^{2+}-bound water is activated to a more nucleophilic hydroxide-like state by the site 2 Zn^{2+} (possibly in conjunction with the site 1 Zn^{2+}) and Asp-255 acting as a general base. This activated water attacks the scissile carbonyl of LV which is polarized by binding interactions with the site 1 Zn^{2+} (Zn-488) and Arg-336. (b) A tetrahedral *gem*-diolate transition state is formed, resulting in a noncovalent enzyme–ligand intermediate. O_a is the *gem*-diolate oxygen which was formerly the scissile carbonyl oxygen of the substrate. O_b is the *gem*-diolate oxygen which was formerly the attacking water. The *gem*-diolate is stabilized by interactions with the active site Zn^{2+}s and Arg-336. Decomposition of this intermediate to products is facilitated by the protonation of the amino group of the leaving L-valine by Lys-262. (c) The original protonation states of the enzymic amino acid residues can be restored by the transfer of the carboxylate proton of Asp-255 to the side chain amino group of Lys-262. The $O_{\delta}1$ carboxylate oxygen of Asp-255 and the N_{ζ} amino nitrogen of Lys-262 are 4.0 Å apart in the blLAP–amastatin structure. Although in this figure the positive charge of the guanidinium group of Arg-336 is depicted as localized to one of the guanidinium nitrogens, this charge is essentially delocalized over all three guanidinium nitrogens.

Figure 12, consistent with its proposed electrophilic role. The side chain amine group of Lys-262, the third named enzymic residue in the proposed mechanism, has a pK_a of ~10. It is likely that neither the protonated nor the unprotonated form of Lys-262 greatly predominates at pH 9. The presumptive protonation lability of the Lys-262 side chain amine at this pH is consistent with its proposed proton shuttling role. There are also some biochemical studies which support the overall general base aspect of the proposed mechanism. α-Aminoaldehydes and α-chloromethylketones have been investigated as reaction coordinate analogue inhibitors of LAP (Andersson et al., 1982, 1985; Frick & Wolfenden, 1985; Birch et al., 1972). The results of these studies indicated that these inhibitors bound noncovalently to the enzyme in their hydrated forms, as would be expected for a general base mechanism, and not covalently to the enzyme, as would be expected for an anhydride mechanism. Studies of the blLAP-catalyzed transpeptidation reaction in $H_2{}^{18}O$ also concluded that blLAP catalysis proceeds through a noncovalently bound enzyme–ligand intermediate, and not a covalently bound one (Antonov et al., 1981).

On the basis of the crystallographically determined binding modes of amastatin and the modeled binding modes of LV and LVTS, the P_1 hydroxyl oxygen of amastatin appears to be the analogue of the attacking water in the present proposed mechanism for blLAP catalysis (Figures 3, 10, and 12). The interactions of the hydroxyl oxygen of amastatin with the enzyme are more like those of the *gem*-diolate O_b oxygen of LVTS than those of the scissile carbonyl oxygen of LV or the *gem*-diolate O_a oxygen of LVTS (Tables II–IV). An aspect of the tight-binding nature of amastatin (or bestatin) appears to be that the interactions of its hydroxyl oxygen with the active site Zn^{2+}s in blLAP mimic the interactions of a metal-bound nucleophilic water and the subsequent *gem*-diolate oxygen of the transition state. The importance of the hydroxyl group in amastatin binding is demonstrated by deoxyamastatin (amastatin minus the C2 hydroxyl group), which binds over three orders of magnitude less tightly to pkLAP than does amastatin (Rich et al., 1984). LV can, however, be modeled in an alternative binding mode, binding mode II, which results in similar binding interactions between the hydroxyl oxygen of amastatin and the scissile carbonyl oxygen of LV (Figure 13). The molecular conformation of LV modeled in either binding mode I or II is constrained by the peptide bond which is in the energetically favorable *trans* conformation. Water attack on the scissile carbonyl carbon of LV in either binding mode could result in the modeled binding mode of the *gem*-diolate transition state LVTS as depicted in Figure 10, since nucleophilic attack on the scissile carbonyl carbon of LV would destroy the conformationally constraining peptide bond. Mechanistically, however, LV binding modes I and II are different in that the scissile carbonyl carbon is accessible to nucleophilic attack by a water from different sides of the active site binding groove in the two modeled binding modes. With respect to the orientation of the active site as depicted in Figure 9, LV modeled in binding mode I would be attacked from the left (Zn^{2+}) side of the active site binding groove. A water launching a nucleophilic attack from this vantage would be in position to be activated by one or both Zn^{2+}s and Asp-255 acting as a general base. Furthermore, in modeled binding mode I, Arg-336 could polarize the scissile carbonyl of LV for nucleophilic attack. In modeled binding mode II, the scissile carbonyl of LV points more toward the Zn^{2+} side of the active site binding groove and away from the Arg-336 side than in modeled binding mode I (Figure 13), making the scissile carbonyl more amenable to nucleophilic attack from the right side of the active site binding groove than from the left. Water

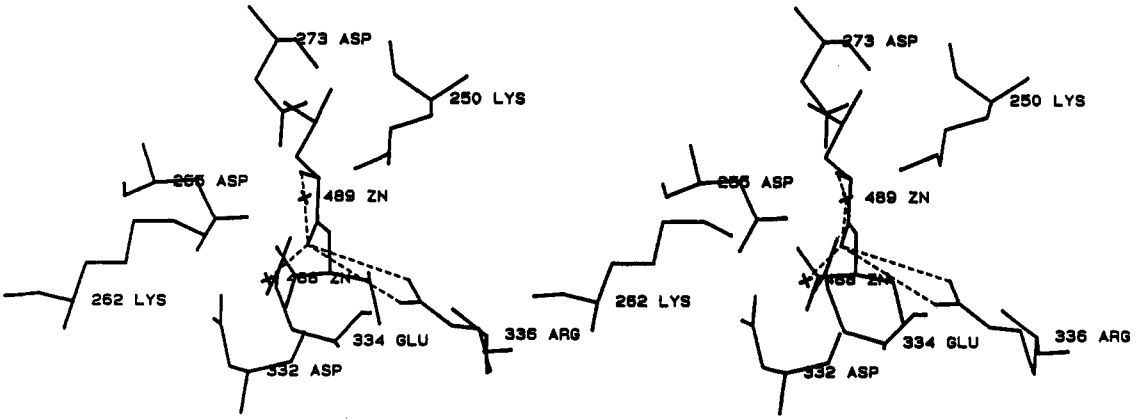

FIGURE 13: Stereoview of LV modeled into the active site of blLAP in binding mode II as described in the text. The coordinates of Lys-250, Asp-255, Lys-262, Asp-273, Asp-332, Glu-334, Arg-336, Zn-488, Zn-489, and LV are shown.

attacking LV from the right side would be in a less favorable position to be activated by the Zn^{2+}s. The *gem*-diolate O_a of LVTS in the modeled blLAP–LVTS complex would represent the attacking water in the blLAP-catalyzed proteolysis of LV in binding mode II (Figure 10). This oxygen is 4.5 Å from both Zn^{2+}s. Additionally, on the right side of the active site, there are no likely enzymic residues which could act as a general base, as Asp-255 could in hydrolysis of LV in binding mode I. The orientation of the scissile carbonyl of LV in binding mode II also appears to be less favorable for a polarizing interaction with the guanidinium group of Arg-336. In formulating a general base mechanism for the hydrolysis of LV, modeled binding mode I appears tobe more consistent with the arrangement of reactive enzymic components than does modeled binding mode II.[5]

The catalytic mechanism proposed herein for blLAP is based on the mechanism which was previously proposed following the determination of the X-ray crystal structure of the blLAP–bestatin complex (Burley et al., 1991). Since the determination of the blLAP–bestatin structure, the X-ray crystallographic identification of the two metal binding sites (Kim & Lipscomb, 1993) and the present determination of the blLAP–amastatin structure, in conjunction with previous biochemical data, have allowed a fuller development of the previously proposed catalytic mechanism for blLAP. Taylor (Taylor et al., 1993) has recently proposed a catalytic mechanism for blLAP based on bestatin inhibition studies. Although this mechanism of Taylor is much like the blLAP–bestatin structure-based mechanism (Burley et al., 1991), there are aspects of the former mechanism which are inconsistent with the structure of blLAP. In the mechanism of Taylor, Zn-489 is assigned to be the more readily exchangeable site 1 metal and is invoked to initiate the reaction and stabilize the tetrahedral intermediate. No catalytic role is proposed for Zn-488. The X-ray crystallographic determination of the structure of the Zn^{2+}–Mg^{2+} metallohybrid blLAP has shown that Zn-489 is in fact the more tightly bound site 2 metal (Kim & Lipscomb, 1993). In addition, it must be stressed that not only our X-ray crystallographic studies but also numerous biochemical studies of LAP have indicated that both metals can have important roles in blLAP catalysis. Furthermore, Arg-336, which appears to be a very important catalytic residue from the X-ray crystal structures of blLAP, is not mentioned in the mechanism of Taylor, except to be invoked in a questionable Zn^{2+} binding role. The depiction of the enzymic Zn^{2+} coordination in the mechanism of Taylor is also inconsistent with X-ray crystallographic studies of blLAP. In the mechanism of Taylor, Glu-334 is depicted to bind both Zn^{2+}s using only one of its side chain carboxylate oxygens, while Asp-332 chelates one of the Zn^{2+}s with both of its side chain carboxylate oxygens. The X-ray crystal structures of blLAP show that both side chain carboxylate oxygens of Glu-334 bind one to each of the Zn^{2+}s, and that only one of the side chain carboxylate oxygens of Asp-332 is within interaction distance of a Zn^{2+} (Zn-488) (Figure 6).

[5] Another possible binding mode for LV is one in which the scissile carbonyl of LV coincides with the P_1 carbonyl of amastatin. Such a binding mode appears to be unproductive since the scissile carbonyl would be far from the catalytically important Zn^{2+}s. The P_1 carbonyl oxygen of amastatin is 3.9 Å from Zn-488 and 5.0 Å from Zn-489. Furthermore, in such a binding mode, as is the case for LV binding mode II, the scissile carbonyl would be accessible to nucleophilic attack by a water from the right side of the active site binding groove, which appears to be less compatible with the arrangement of reactive enzymic components than does water attack from the left side.

ACKNOWLEDGMENTS

We acknowledge Prof. A. Taylor for assistance in early isolations of blLAP and Prof. J. E. Gouaux for helpful advice on the purification of blLAP. We thank Prof. S. K. Burley for excellent discussions on blLAP.

REFERENCES

Allen, M. P., Yamada, A. H., & Carpenter, F. H. (1983) *Biochemistry 22*, 3778–3783.

Andersson, L., Isley, T. C., & Wolfenden, R. (1982) *Biochemistry 21*, 4177–4180.

Andersson, L., MacNeela, J., & Wolfenden, R. (1985) *Biochemistry 24*, 330–333.

Aoyagi, T., Tobe, H., Kojima, F., Hamada, M., Takeuchi, T., & Umezawa, H. (1978) *J. Antibiot. 31*, 636–638.

Birch, P. L., El-Obeid, H. A., & Akhtar, M. (1972) *Arch. Biochem. Biophys. 148*, 447–451.

Blum, M., Metcalf, P., Harrison, S. C., & Wiley, D. C. (1987) *J. Appl. Crystallogr. 20*, 235–242.

Blow, D. M. (1976) *Acc. Chem. Res. 9*, 145–152.

Brünger, A. T. (1990) *X-PLOR Manual*, Version 2.1, Yale University, New Haven, CT.

Brünger, A. T., Kuriyan, J., & Karplus, M. (1987) *Science 235*, 458–460.

Burley, S. K., David, P. R., Taylor, A., & Lipscomb, W. N. (1990) *Proc. Natl. Acad. Sci. U.S.A. 87*, 6878–6882.

Burley, S. K., David, P. R., & Lipscomb, W. N. (1991) *Proc. Natl. Acad. Sci. U.S.A. 88*, 6916–6920.

Burley, S. K., David, P. R., Sweet, R. M., Taylor, A., & Lipscomb, W. N. (1992) *J. Mol. Biol. 224*, 113–140.

Carpenter, F. H., & Vahl, J. M. (1973) *J. Biol. Chem. 248*, 294–304.

Christianson, D. W., & Lipscomb, W. N. (1989) *Acc. Chem. Res. 22*, 62–69.
Cuypers, H. T., van Loon-Klaassen, L. A. H., Vree Egberts, W. T. M., de Jong, W. W., & Bloemendal, H. (1982) *J. Biol. Chem. 257*, 7077–7085.
David, P. R. (1991) Ph.D. Thesis, Harvard University, Cambridge, MA.
Delange, R. J., & Smith, E. L. (1971) *Enzymes (3rd ed.) 3*, 81–118.
Eichele, G., Ford, G. C., & Jansonius, J. N. (1979) *J. Mol. Biol. 135*, 513–516.
Frick, L., & Wolfenden, R. (1985) *Biochim. Biophys. Acta 829*, 311–318.
Gordon, E. M., Godfrey, J. D., Delaney, N. G., Asaad, M. M., Von Langen, D., & Cushman, D. W. (1988) *J. Med. Chem. 31*, 2199–2211.
Groves, J. T., & Olson, J. R. (1985) *Inorg. Chem. 24*, 2715–2717.
Hanson, H., & Frohne, M. (1976) *Methods Enzymol. 45*, 504–521.
Harbeson, S. L., & Rich, D. H. (1988) *Biochemistry 27*, 7301–7310.
Himmelhoch, S. R. (1969) *Arch. Biochem. Biophys. 134*, 597–602.
Jones, T. A. (1985) *Methods Enzymol. 115*, 157–171.
Jurnak, F., Rich, A., van Loon-Klaassen, L., Bloemendal, H., Taylor, A., & Carpenter, F. H. (1977) *J. Mol. Biol. 112*, 149–153.
Kim, H., & Lipscomb, W. N. (1991) *Biochemistry 30*, 8171–8180.
Kim, H., & Lipscomb, W. N. (1993) *Proc. Natl. Acad. Sci. U.S.A. 90*, 5006–5010.
Kim, H., Burley, S. K., & Lipscomb, W. N. (1993) *J. Mol. Biol. 230*, 722–724.
Lin, W.-Y., Lin, S. H., & Van Wart, H. E. (1988a) *Biochemistry 27*, 5062–5068.
Lin, W.-Y., Lin, S. H., Morris, R. J., & Van Wart, H. E. (1988b) *Biochemistry 27*, 5068–5074.
Lipscomb, W. N. (1970) *Acc. Chem. Res. 3*, 81–89.
Long, C. (1961) *Biochemists' Handbook*, E. & F. N. Spon, Ltd., London.
Luzatti, P. V. (1952) *Acta Crystallogr. 5*, 802–810.
Matthews, B. W. (1988) *Acc. Chem. Res. 21*, 333–340.
Melbye, S. W., & Carpenter, F. H. (1971) *J. Biol. Chem. 246*, 2459–2463.
Nishino, N., & Powers, J. C. (1979) *Biochemistry 18*, 4340–4347.
Nishizawa, R., Saino, T., Takita, T., Suda, H., Aoyagi, T., & Umezawa, H. (1977) *J. Med. Chem. 20*, 510–515.
Ocain, T. D., & Rich, D. H. (1988) *J. Med. Chem. 31*, 2193–2199.
Petsko, G. A. (1975) *J. Mol. Biol. 96*, 381–392.
Rees, D. C., Lewis, M., & Lipscomb, W. N. (1983) *J. Mol. Biol. 168*, 367–387.
Ricci, J. S., Jr., Bousvaros, A., & Taylor, A. (1982) *J. Org. Chem. 47*, 3063–3065.
Rich, D. H., Moon, B. J., & Harbeson, S. (1984) *J. Med. Chem. 27*, 417–422.
Sander, C., & Schneider, R. (1991) *Proteins 9*, 56–68.
Schechter, I., & Berger, A. (1967) *Biochem. Biophys. Res. Commun. 27*, 157–162.
Shen, C., & Melius, P. (1977) *Prep. Biochem. 7*, 243–256.
Smith, E. L., & Spackman, D. H. (1955) *J. Biol. Chem. 212*, 271.
Stirling, C. J., Stewart, G., & Sherratt, D. J. (1988) *Mol. Gen. Genet. 214*, 80–84.
Stirling, C. J., Colloms, S. D., Collins, J. F., Szatmari, G., & Sherratt, D. J. (1989) *EMBO J. 8*, 1623–1627.
Sweet, R. M., Wright, H. T., Janin, J., Chothia, C. H., & Blow, D. M. (1974) *Biochemistry 13*, 4212–4228.
Taylor, A., Surgenor, T., Thomson, D. K. R., Graham, R. J., & Oettgen, H. (1984a) *Exp. Eye Res. 38*, 217–229.
Taylor, A., Volz, K. W., Lipscomb, W. N. & Takemoto, L. J. (1984b) *J. Biol. Chem. 259*, 14757–14761.
Taylor, A., Peltier, C. Z., Jahngen, E. G. E., Jr., Laxman, E., Szewczuk, Z., & Torre, F. J. (1992) *Biochemistry 31*, 4141–4150.
Taylor, A., Peltier, C. Z., Torre, F. J., & Hakamian, N. (1993) *Biochemistry 32*, 784–790.
Teng, T.-Y. (1990) *J. Appl. Crystallogr. 23*, 387–391.
Thaller, C., Weaver, L. H., Eichele, G., Wilson, E., Karlsson, R., & Jansonius, J. N. (1981) *J. Mol. Biol. 147*, 465–469.
Thompson, G. A., & Carpenter, F. H. (1976) *J. Biol. Chem. 251*, 1618–1624.
Tilton, R. F., Jr., Dewan, J. C., & Petsko, G. A. (1992) *Biochemistry 31*, 2469–2481.
Turzynski, A., & Mentlein, R. (1990) *Eur. J. Biochem. 190*, 509–515.
Umezawa, H., Aoyagi, T., Suda, H., Hamada, M., & Takeuchi, T. (1976) *J. Antibiot. 29*, 97–99.
Van Wart, H. E., & Lin, S. H. (1981) *Biochemistry 20*, 5682–5689.
Van Wart, H. E., & Lin, S. H. (1983) *Proc. Natl. Acad. Sci. U.S.A. 80*, 7506–7509.
Vogt, V. (1970) *J. Biol. Chem. 245*, 4760–4769.
Wagstaffe, P. J., Hecht, H., Muntau, H., & Schramel, P. (1987) *Fresenius' Z. Anal. Chem. 329*, 475–479.
Wilkes, S. H., & Prescott, J. M. (1985) *J. Biol. Chem. 260*, 13154–13162.
Zhang, Y., Liang, J.-Y., Huang, S., Ke, H., & Lipscomb, W. N. (1993) *Biochemistry 32*, 1844–1857.